tvst

Article

Modeling Cone/Cone–Rod Dystrophy Pathology by AAV-Mediated Overexpression of Mutant CRX Protein in the Mouse Retina

Yuwei Wang[1,2,*], Xiaomeng Li[1,2,*], Yang Yu[1,*], Jian Liang[1,2], Yang Liu[1,2], Yuhong Chen[1,2], Xinyue Bai[1,2], Jieqiong Chen[1,2], Fenghua Wang[1–4], Xueting Luo[1–3], and Xiaodong Sun[1–4]

[1] Department of Ophthalmology, Shanghai General Hospital, Shanghai Jiao Tong University School of Medicine, Shanghai, China
[2] Shanghai Key Laboratory of Fundus Diseases, Shanghai, China
[3] National Clinical Research Center for Eye Diseases, Shanghai, China
[4] Shanghai Engineering Center for Visual Science and Photomedicine, Shanghai, China

Correspondence: Xiaodong Sun and Xueting Luo, Department of Ophthalmology, Shanghai General Hospital, Shanghai Jiao Tong University School of Medicine, 100 Haining Rd, Shanghai 200080, China. xdsun@sjtu.edu.cn; xuetingluo@126.com

Received: October 10, 2020
Accepted: February 26, 2021
Published: June 18, 2021

Keywords: cone/cone–rod dystrophy; animal model; adeno-associated virus; *CRX* mutation; inherited retinal dystrophies

Citation: Wang Y, Li X, Yu Y, Liang J, Liu Y, Chen Y, Bai X, Chen J, Wang F, Luo X, Sun X. Modeling cone/cone–rod dystrophy pathology by AAV-mediated overexpression of mutant CRX protein in the mouse retina. Transl Vis Sci Technol. 2021;10(7):25, https://doi.org/10.1167/tvst.10.7.25

Purpose: This study aims to evaluate the pathogenesis of cone/cone–rod dystrophy (CoD/CoRD) caused by a *cone–rod homeobox (CRX)* mutation, which was identified in a Chinese family, through adeno-associated virus (AAV)-mediated overexpression of mutant CRX protein in the mouse retina.

Methods: Comprehensive ophthalmologic examinations were performed for the pedigree members of a Chinese family with CoD/CoRD. Whole exome sequencing and Sanger sequencing were performed to determine the genetic cause of the disease. Furthermore, AAV vectors were used to construct AAV-CRX-mut-HA, which was transfected into mouse photoreceptor cells to clarify the pathogenesis of the mutant CRX.

Results: Fundus photography and optical coherence tomography images displayed features that were consistent with CoD/CoRD, including macular atrophy and photoreceptor layer thinning. Electroretinogram analysis indicated an obvious decrease in photopic responses or both scotopic and photopic responses in affected individuals. A frameshift variant c.611delC (p.S204fs) in *CRX* was cosegregated with the disease in this family. AAV-CRX-mut-HA that subretinally injected into the C57BL/6 mice generally transfected the outer nuclear layer, leading to the loss of cone and rod photoreceptor cells, abnormal expression of CRX target genes, and a decrease in electroretinogram responses.

Conclusions: AAV-mediated overexpression of CRX$^{[S204fs]}$ in the mouse retina led to a CoRD-like phenotype and showed the possible pathogenesis of the antimorphic CRX mutation.

Translational Relevance: This study provides a modeling method to evaluate the pathogenesis of CoD/CoRD and other inherited retinal dystrophies caused by distinct gain-of-function mutations.

Introduction

Cone/cone–rod dystrophies (CoD/CoRD) are severe forms of inherited retinal dystrophies characterized by progressive cone dysfunction, primarily manifesting as a loss of central visual acuity, abnormal color vision, and photopia.[1,2] For CORD, this is followed by nyctalopia and peripheral visual field loss caused by loss of rod photoreceptor cells. CoD and CoRD are the most common cause of hereditary cone dysfunction, with a prevalence ranging from 1:30,000 to 1:40,000.[3,4]

There is significant genotypic and phenotypic variability implicated in CoD/CoRD. Currently, mutations in 32 genes are reported to cause COD or CORD, and mainly affect photoreceptor structure and function.[5] The lack of model systems that adequately mimic the diverse genotypic and phenotypic characteristics is a significant impediment to the development of understanding and therapies for CoD/CoRD. In vitro experiments facilitate investigating the structure and function of the mutant protein to some extent, but from which the in vivo impact cannot be inferred with confidence. Mostly, transgenic animal models carrying distinct mutations were established to observe the progression of the disease and unravel the underlying molecular genetic basis.[6–8] Take *CRX* as an example, which encodes a "paired-like" homeodomain transcription factor essential for the development and survival of photoreceptors,[9,10] and accounts for about 15.6% of autosomal-dominant CoD/CoRD cases. Crx^{E168d2} knock-in mice carried the frameshift deletion p.E168d2, generating the truncated CRX protein that failed to transactivate the target genes,[8,11] and modeled early-onset CoRD or Leber congenital amaurosis. However, the high technical difficulties and high cost of establishing an animal model carrying a specific pathogenic mutation make it unavailable in most conditions. Therefore, as for a potential pathogenic variant found in clinical practice, it is significant to establish a reliable and feasible animal model to confirm its pathogenicity and explore the underlying mechanism.

Adeno-associated virus (AAV)-mediated gene transfer has always served as a therapeutic method for rescuing retinal function for inherent retinal diseases,[12,13] since the first gene therapy drug, an AAV2/2 vector carrying *RPE65* gene for the treatment of *RPE65*-associated retinitis pigmentosa or Leber congenital amaurosis reached the market.[14] AAV vectors are most commonly used due to their high transduction efficiency and excellent safety profile. Actually, AAV-mediated gene overexpression is not only used for gene therapy, but also for establishing animal models to study the pathogenic effects of the proteins.[15–17] Given that most *CRX* mutations act through antimorphic mechanism (a type of gain-of-function mutation),[18] we delivered an AAV vector expressing the mutant CRX the same as the patients by subretinal injection in wild-type (WT) mice, to evaluate the phenotype and analyze pathogenesis of the mutation. We aimed to develop a novel animal model by AAV-mediated gene delivery and provide a systematic process to evaluate the pathogenic variant, from clinical and genetic analysis to confirmation using an animal model.

Methods

Patients and Clinical Examination

This observational study followed the tenets of the Declaration of Helsinki. Informed consent was obtained after the study risks and benefits were thoroughly explained. The family and medical history of all the subjects were collected. Three affected and an unaffected individual of the family underwent a standardized ophthalmologic examination, including best-corrected visual acuity by Snellen visual acuity, color vision by Ishihara test, refraction, and fundoscopy. The presence of nystagmus was evaluated qualitatively. Retinal imaging included color fundus photography (Visucam 200 digital fundus camera, Carl Zeiss Meditec, Dublin, CA), spectral-domain optical coherence tomography (OCT), and fundus autofluorescence (FAF) imaging (both from Spectralis, Heidelberg Engineering, Germany). A full-field electroretinogram (ERG, RETIport, Roland Consult, Brandenburg, Germany) was performed according to the International Society for Clinical and Electrophysiology of Vision standards.

Whole Exome Sequencing and Sanger Confirmation

The peripheral blood sample of the proband was collected for whole exome sequencing as previously described.[19] The functional effect of the candidate mutations was predicted with 3 commonly used tools: PolyPhen 2 (http://genetics.bwh.harvard.edu/pph2/), SIFT (http://sift.jcvi.org/), and MutationTaster (http://www.mutationtaster.org/).

Sanger sequencing was performed in other available pedigree members to validate the cosegregation of the *CRX* variant through the pedigree (Fig. 1). The genomic fragment surrounding the candidate mutation was amplified with a pair of primers: 5′- CCCAAGACCCTCCACAGATG-3′ and 5′-ATCAGGTCTCCCAGGTACCC-3′. Sanger sequencing was used for targeted mutation screening after polymerase chain reaction (PCR) amplification.

Plasmid Construction and AAV Production

The human *CRX* (NM_000554) complementary DNA was amplified by PCR with primers 5′-ACTGAATTCCGCGGGCCCGGCCACCATGATG GCGTATATGAAC-3′ and 5′-GATCGCAGGTGA GGCCTAGCTAAGCGTAATCTGGAACATCGTA TGGGTACAAGATCTGAAACTTCC-3′. The 611

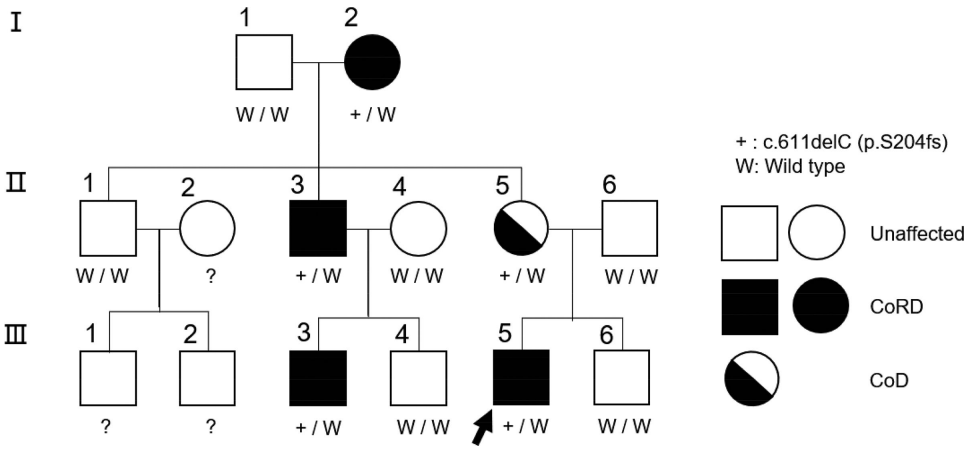

Figure 1. Pedigree. The arrow indicates the proband.

delC deletion mutation was introduced by PCR with primers 5′- ACTGAATTCCGCGGGCCCGGCCACCATGATGGCGTATATGAAC - 3 ′ and 5′ - GATCGCAGGTGAGGCCTAGCTAAGCGTAATCTGGAACATCGTATGGGTAGGCCGCTGAAATAGGAGC-3′. The PCR products of *CRX* followed by an HA tag were subcloned into the AAV-green fluorescent protein (GFP) vector (Addgene #32396) with a cytomegalovirus promoter, and substituted for GFP to generate AAV-CRX-wt-HA and AAV-CRX-mut-HA constructs. The Sanger sequencing was carried out for the verification of plasmid constructs.

AAVs were produced by transfection of HEK 293T cells (CRL-11268) with pAAV-RC plasmid, pHelper (Agilent Technologies, CA), and either AAV-CRX-wt-HA, AAV-CRX-mut-HA, or AAV-GFP in a 1:2:1 ratio. Viral titers were approximately 1×10^{13} vg/mL.

Subretinal Delivery of AAV Constructs

All animal experiments were conducted in accordance with the ARVO Statement for the Use of Animals in Ophthalmic and Vision Research. The delivery of AAV constructs into mouse photoreceptors was achieved by subretinal injections.[20] Three-week-old C57BL/6 WT mice were anesthetized with chloral hydrate (350 mg/kg intraperitoneally). After dilation with 0.5% tropicamide for 10 minutes, the eyes were gently protruded and covered with a drop of 0.3% ofloxacin oculentum (Shenyang, China) as a hemispherical magnifying lens. A tunnel was created with a sharp 30G needle puncturing adjacent to the limbus. Then, 1 µL of AAV-CRX-mut-HA for the right eye and AAV-CRX-wt-HA or AAV-GFP as control vectors for the left eye were injected slowly into the subretinal space using a blunt 34G needle through the same scleral hole. The mark of a successful injection was the presence of a small bubble.

Immunofluorescence Analysis

Immunofluorescence analysis was performed with mouse retinal sections. Cryosections were prepared as described previously.[21] After fixation and blocking, primary antibodies used for staining were rat anti-HA (1:500, AF0039, Beyotime), chicken anti-GFP (1:500, ab13970, Abcam, Cambridge, MA), rabbit anti-Rhodopsin (RHO) (1:500, 1D4, Santa Cruz Biotechnology, Santa Cruz, CA), and rabbit anti-cone arrestin (1:500, AB15282, Merck Millipore, Billerica, MA). The samples were washed and then stained at room temperature for 1 hour with Alexa Fluor 594- and 488-conjugated secondary antibodies (1:1000, Proteintech). As for the quantification of RHO and cone arrestin, six sections each with six random fields were captured and measured by a masked observer.

Western Blot Analysis

The affected retinas were dissolved with radioimmunoprecipitation assay buffer (P0013C, Beyotime, Shanghai, China) containing protease inhibitors. Samples were subjected to 10% SDS-PAGE gels then transferred to polyvinylidene difluoride membranes (IPFL00010, Merck Millipore). The membranes were blocked by 5% skim milk in TRIS-buffered saline TWEEN-20 for 2 hours at room temperature, followed by probed with primary antibodies for GAPDH (1:1000, 10494-1-AP, Proteintech, Chicago, IL) and HA (1:1000, AF0039, Beyotime, Shanghai, China). The membranes were then incubated with secondary antibodies (1:2000, SA00006-4, Proteintech) for 1 hour

Table 1. Quantitative RT-PCR Primers

Gene	Forward Primer	Reverse Primer
Mouse RHO	GCTTCCCTACGCCAGTGTG	CAGTGGATTCTTGCCGCAG
Mouse GNAT1	GATGCCCGCACTGTGAAAC	CCAGCGAATACCCGTCCTG
Mouse GNAT2	GGATGGCTACTCACCCGAAG	TGCATAGTCAATGCCTAGTGTG
Mouse ARR3	AAGTTTTCCATCTACCTGGGG	TCACATCCAAGTCATCACGG
Mouse OPN1SW	GCTGGACTTACGGCTTGTCACC	TGTGGCGTTGTGTTTGCTGC
Mouse OPN1MW	GGTGGTGATGGTCTTCGCATAC	TTGGAGGTGCTGGAAAGTTCAG
Mouse RBP3	ATGAGAGAATGGGTCCTGGTT	GCCCAGAATCTCGTGACTCTTC
Mouse CRX	GTTCAAGAATCGTAGGGCGAA	TGAGATGCCCAAAGGATCTGT
Human CRX	GGGTTCAGGTTTGGTTCAAGA	GGTCTGGACACACATCTGTGG

at room temperature, and visualized using a molecular imager (Amersham Imager 600, GE Healthcare, Buckinghamshire, UK).

Real-Time Quantitative PCR

The extracted total RNA from retinas with a Total RNA Extraction Kit (DP419, Tiangen, Beijing, China) were quantified using NanoDrop 2000c spectrophotometer (Thermo Fisher Scientific, Wilmington, DE). RT Master Mix (Takara Bio Inc., Dalian, China) was used to generate complementary DNA. The real-time quantitative PCR was performed using SYBR Premix Ex Taq (DRR041A, Takara, Dalian, China) following the manufacturer's protocol. The primer sequences are listed in Table 1.

OCT Imaging

In vivo retinal imaging in mice was captured using the Phoenix mouse OCT2 system (Phoenix Research Labs, Pleasanton, CA) 4 weeks after subretinal injection. Anesthetization and pupil dilation was performed as described above. The scan of the central retina across the optic nerve head was selected for the measurement of outer nuclear layer (ONL) thickness. We measured the thickness at a standard distance of 400 µm from the optic nerve head.

TUNEL Staining

TUNEL staining was used to assess apoptosis in retinal sections using the In Situ Cell Death Detection Kit (11684795910, Roche Diagnostics, Mannheim, Germany) according to the manufacturer's protocol. Sections were counterstained with DAPI-blue.

ERG Recordings

The mouse full-field ERG was recorded using a scotopic Ganzfeld ERG system (Phoenix Research Labs). After dark adaption overnight, mice were anesthetized and pupils were dilated with atropine as mentioned elsewhere in this article. A small amount of 0.3% of ofloxacin oculentum was applied to the surface of the eyes to establish contact between the cornea and the electrode. The reference needle electrode was placed behind the ears, and a needle electrode midway up the tail served as the ground electrode. Dark-ERG was performed at six stimulus intensities (–0.5, 0.0, 0.5, 1.0, 1.5, and 2.0 log cd·s/m^2). For stimulus intensities varying from –0.5 to 0.5 log cd·s/m^2, the interstimulus interval was 1 second; and for stimulus intensities of 1 to 2 log cd·s/m^2, the interstimulus interval was 10 seconds. The mice were light-adapted with a background illumination of 25 cd/m^2 for 10 minutes, and then subjected to photopic measurements obtained at 0, 1, 2, and 3 log cd·s/m^2 with a 10-second interstimulus interval. A-wave and b-wave amplitudes of dark-adapted and light-adapted responses were determined with five individual recordings average for each measurement.

Statistical Analysis

Data were shown as mean ± standard error of the mean. Data analysis and graphic representation were performed using the GraphPad Prism 8.0 software (San Diego, CA). The mouse ERG recordings were analyzed using repeated measures two-way analysis of variance tests, with AAV vectors and stimulus intensity as factors, were used to compare responses between the CRX-wt-HA and CRX-mut-HA groups. The other experiments were repeated in triplicate. Differences between the two groups were determined by the unpaired two-tailed Student *t*-test.

P values of less than 0.05 were considered statistically significant.

Results

Clinical Features

The pedigree is shown in Figure 1. Clinical data of four members are summarized in Table 2. The proband (Fig. 1, IV:5), a 16-year-old boy, claimed photophobia, nyctalopia, and color vision defects when he came to the clinic, and visual acuity was 0.05 bilaterally with no significant improvement with spectacles. Fundus photography displayed a slight pallor of the optic disc color, a thinning artery, pigmentation disorder in the posterior pole, and disappearance of the central foveal reflex (Fig. 2A). FAF revealed mild hypofluorescent lesions near the fundus vascular arch and a surrounding hyperfluorescent ring (Fig. 2A). Through OCT imaging, prominent outer retinal layer atrophy, retinal pigment epithelial atrophy, disappeared ellipsoid zone, paracentral disrupted interdigitation zone, and choroidal structural changes were noticed in both eyes (Fig. 2A). An ERG analysis of proband demonstrated a severe decrease in photopic responses and mild decrease in scotopic responses, supporting a diagnosis of CoRD (Fig. 2E).

Furthermore, we were able to assess three additional individuals from this family, including two affected and one unaffected member. Patient I-2, the 61-year-old grandmother of patient III-5, noticed a decrease of central vision and subsequent nyctalopia in her 40s. Bilaterally, macular dystrophy was observed through fundus examination, and FAF displayed that the peripheral region was also involved (Fig. 2B). In addition, OCT showed severe atrophy and loss of structural integrity in the macular area including the ellipsoid zone (Fig. 2B). We found that the rod response was preserved in the right eye and slightly decreased in the left, and the cone response was notably decreased bilaterally (Fig. 2E). The phenotype of patient I-2 was consistent with a diagnosis of CoRD. Patient II-5, the 36-year-old mother of the proband, presented a progressive decrease in vision in her 20s. Fundus photography, FAF, and OCT images were similar to I-2 with a smaller affected area (Fig. 2C). An ERG analysis revealed preserved rod response and slight decrease in the cone response, leading to a diagnosis of CoD (Fig. 2E). No abnormality was seen in the retinal structure and function of proband's father (II-6) (Figs. 2D, 2E).

Identification of *CRX* Mutation

The whole exome sequencing for the proband revealed a heterozygous deletion mutation c.611delC (p.S204fs) in exon 4 of the *CRX* gene. Disease segregation analysis showed that all affected members had a heterozygous c.611delC (p.S204fs) mutation, and neither mutation was reported in normal relatives (Fig. 3A). The deletion of a cytosine resulted in a frameshift and a premature termination codon at codon 218, producing a protein $CRX^{[S204fs]}$ with a shortened transactivation domain (Fig. 3B).

Subretinal Delivery of AAV-CRX-mut-HA Results in Truncated and Overexpressed $CRX^{[S204fs]}$ in Mouse Photoreceptors

CRX plays an essential role in both the development and maintenance of mammalian rod and cone photoreceptors and is continuously expressed in mature photoreceptor cells. To assess the effect of $CRX^{[S204fs]}$ protein on the maintenance of retinal structure and function, AAV-GFP, AAV-CRX-wt-HA, and AAV-CRX-mut-HA were injected subretinally into C57BL/6 WT mice. After 4 weeks, immunofluorescence assays showed that the outer retina was generally transfected by AAV constructs (Fig. 4A). HA-labeled $CRX^{[S204fs]}$ was distributed in the nucleus as same as normal CRX, suggesting the c.611delC variant had no impact on the subcellular location of CRX (Fig. 4A). Quantitative Western blots assay showed the mutation produced an approximately 36 kD truncated protein with a higher expression level than WT CRX (Fig. 4B). Next, we investigated the expression of exogenous human CRX compared with mouse CRX at the messenger RNA (mRNA) level. The exogenous human CRX mRNA was lower than mouse CRX mRNA both in the CRX-wt-HA and CRX-mut-HA group. Furthermore, mutant human CRX mRNA was significantly more than WT CRX consistent with Western blot results (Fig. 4C). We performed OCT imaging to visualize the retinal structure. No abnormal structure was observed in the GFP and CRX-wt-HA group. The mice injected with the mutant CRX displayed significantly decreased ONL thickness and indistinguishability of inner segment/outer segment (OS) and external limiting membrane (Fig. 4D). Furthermore, apoptosis-mediated photoreceptor loss was evaluated with terminal uridine nick-end labeling (TUNEL) staining (Fig. 4E). A large number of TUNEL-positive cells were observed in the ONL transfected by mutant CRX compared with WT CRX.

Table 2. Clinical Characteristics of the Patients (III-5, I-1, II-5) and the Unaffected Member (II-6)

ID	Disease Status	Age (y); Sex	Symptoms Onset (Age)	Nyctalopia	Photophobia	Dyschromatopsia	Nystagmus	Visual Acuity (OD; OS)	Refraction (OD; OS)	ERG
III-5 (Proband)	Affected	16; Male	Va↓, nyctalopia (12)	+	+	+	−	20/400; 20/400	−3.50 DS/−0.50 DC × 20°; −2.00 DS/−1.50 DC × 160°	Moderately decreased scotopic amplitudes with delayed implicit time, severely decreased photopic amplitudes OU
I-2	Affected	61; Female	Va↓, (∼40)	+	+	+	+	20/333; 20/400	−1.50 DS/−0.75 DC × 50°; −1.00 DS/−0.50 DC × 110°	Mildly decreased scotopic amplitudes with delayed implicit time, severely decreased photopic amplitudes OU
II-5	Affected	36; Female	Va↓, (∼25)	−	+	+	−	20/200; 20/400	−3.75 DS/−1.75 DC × 115°; −4.00 DS/−1.50 DC × 95°	Normal scotopic amplitudes with delayed implicit time, moderately decreased photopic amplitudes OU
II-6	Normal	37; Male	NA	−	−	−	−	20/20; 20/20	Normal	Normal

NA, not applicable.

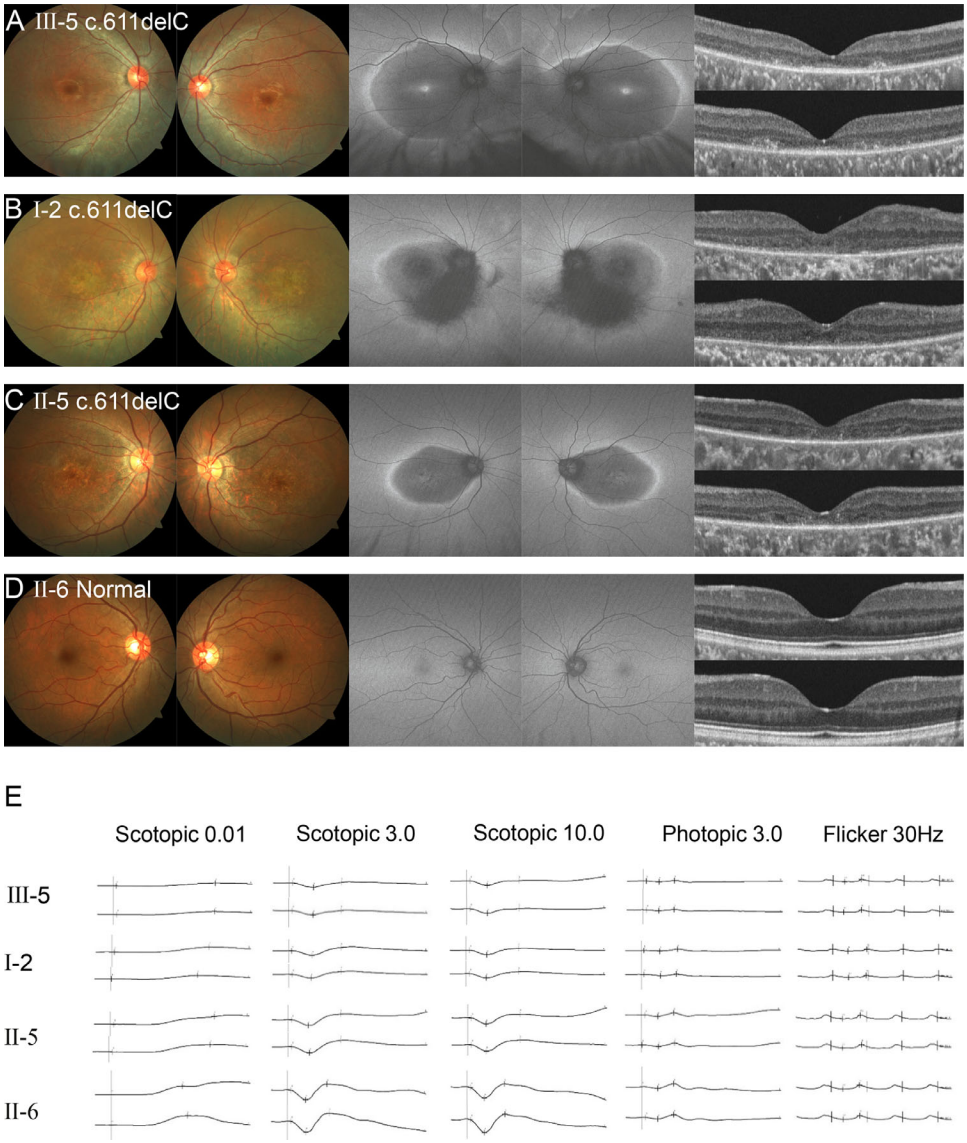

Figure 2. Ophthalmologic examinations of the pedigree members. (A) Patient III-5, the proband. Fundus displayed macular atrophy and absent foveal reflex. FAF revealed mild hypofluorescent lesions with a surrounding hyperfluorescent ring. OCT images showed prominent outer retinal layer and RPE atrophy, paracentrally disrupted interdigitation zone, and abnormal choroidal structures. (B) Patient I-2. Macular dystrophy was observed through fundus examination. FAF displayed the involved peripheral region. OCT showed severe macular atrophy and loss of the ellipsoid zone. (C) Retinal images of patient II-5 were similar to that of her mother I-2 with a smaller affected area. (D) II-6 was an unaffected control. (E) ERG analysis of the four. ERGs of III-5 and I-2 revealed bilaterally reduced scotopic amplitudes with delayed implicit time and severely reduced photopic amplitudes. ERGs of II-5 showed normal scotopic amplitudes with delayed implicit time and reduced photopic amplitudes. II-6 served as normal control. Two traces per person represent the two eyes.

Subretinal Delivery of AAV-CRX-mut-HA Impairs the Expression of Target Photoreceptor Genes

For CRX functions as a transcription factor, several target genes of CRX were assessed using real-time quantitative PCR to verify the transactivation function of mutant CRX protein. Compared with AAV-GFP controls, CRX targets were not changed in the retinas transfected by AAV-CRX-wt-HA, but significantly decreased in those transfected by AAV-CRX-mut-HA (Fig. 5A). Given that the decrease in these transcripts might be due to the loss of ONL cells, we performed the immunofluorescent assay for RHO and cone arrestin on retinal sections to observe the morphology and distribution of the target genes. The $CRX^{[S204fs]}$ protein led to the loss of RHO staining, suggesting the decreased OS length with an abnormal

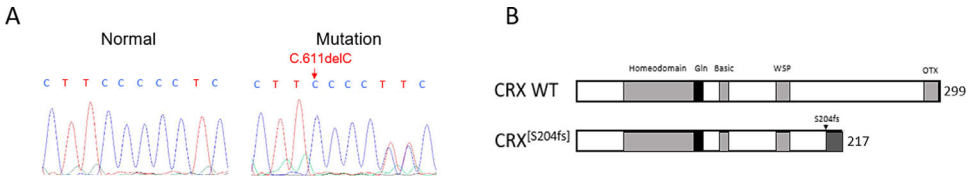

Figure 3. A heterozygous deletion mutation c.611delC (p.S204fs) in exon 4 of CRX was identified as a disease-causing mutation. (A) The affected members showed heterozygous c.611delC (p.S204fs), and neither mutation was reported in normal relatives. (B) Schematic diagram of WT and mutant CRX proteins.

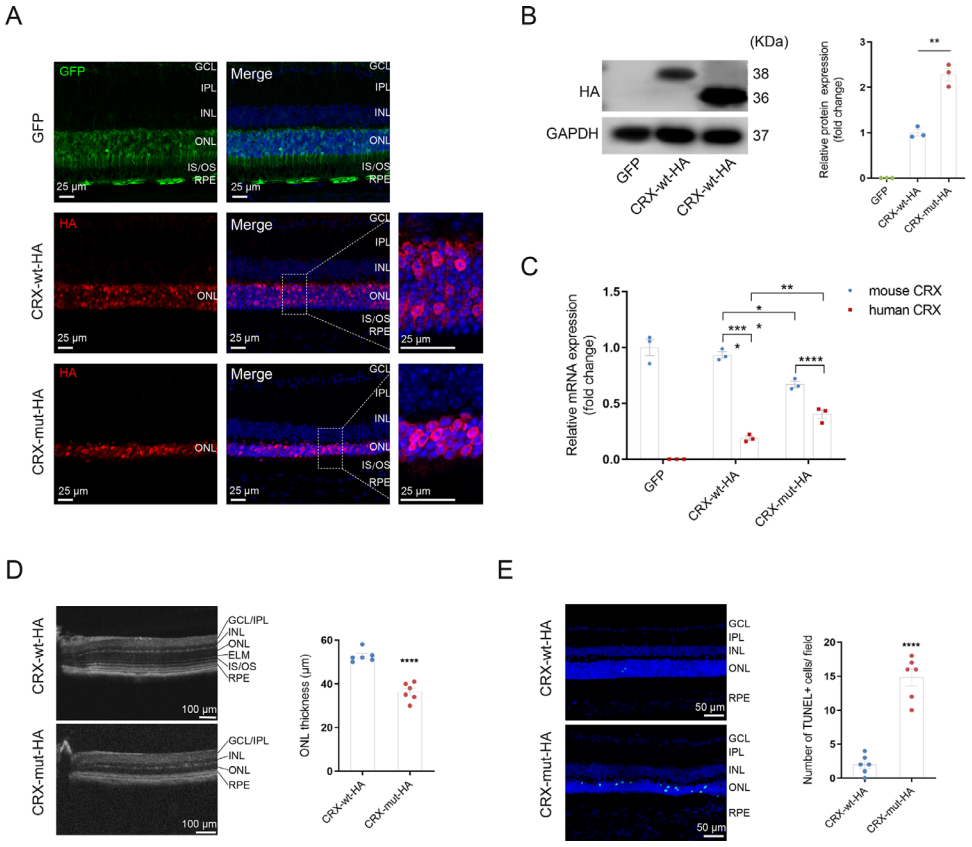

Figure 4. Subretinal delivery of AAV-CRX-wt-HA or AAV-CRX-mut-HA in WT mice. (A) Immunofluorescence assays showed that the ONL was generally transfected by AAV constructs. The magnified portion showed the mutant CRX was predominantly located in the nuclear periphery and partly in the center as same as the WT CRX. (B) Western blot of HA-tagged CRX protein showed overexpression of a truncated mutant CRX compared with HA-tagged WT CRX. (C) At the mRNA level, the exogenous human CRX was lower than endogenous mouse CRX both in the CRX-wt-HA and CRX-mut-HA group. In addition, mutant human CRX mRNA was significantly more than WT CRX. (D) OCT imaging revealed that the mice injected with the mutant CRX showed a significant reduction of ONL thickness and indistinguishability of the ELM and IS/OS. E) TUNEL-positive cells were increased in the ONL transfected by mutant CRX compared with WT CRX ($n = 10$). $^{**}P < 0.01$, $^{***}P < 0.001$, $^{****}P < 0.0001$. GCL, ganglion cell layer; IPL, inner plexiform layer; INL, inner nuclear layer; IS/OS, inner segment/outer segment; RPE, retinal pigment epithelium; ELM, external limiting membrane.

structure (Fig. 5B). Immunostaining of RHO and cone arrestin revealed decreased cones and mislocalized cone nuclei to the inner ONL, implying the abnormal quantity and migration of cone photoreceptors (Fig. 5B). Immunofluorescent staining reflected that the structure of rod and cone photoreceptors were both impaired.

Subretinal Delivery of AAV-CRX-mut-HA Leads to Functional Disorders of Mouse Photoreceptors

To assess the consequence of these morphologic changes on retinal function, we quantified rod and cone light responses 4 weeks after AAV injection

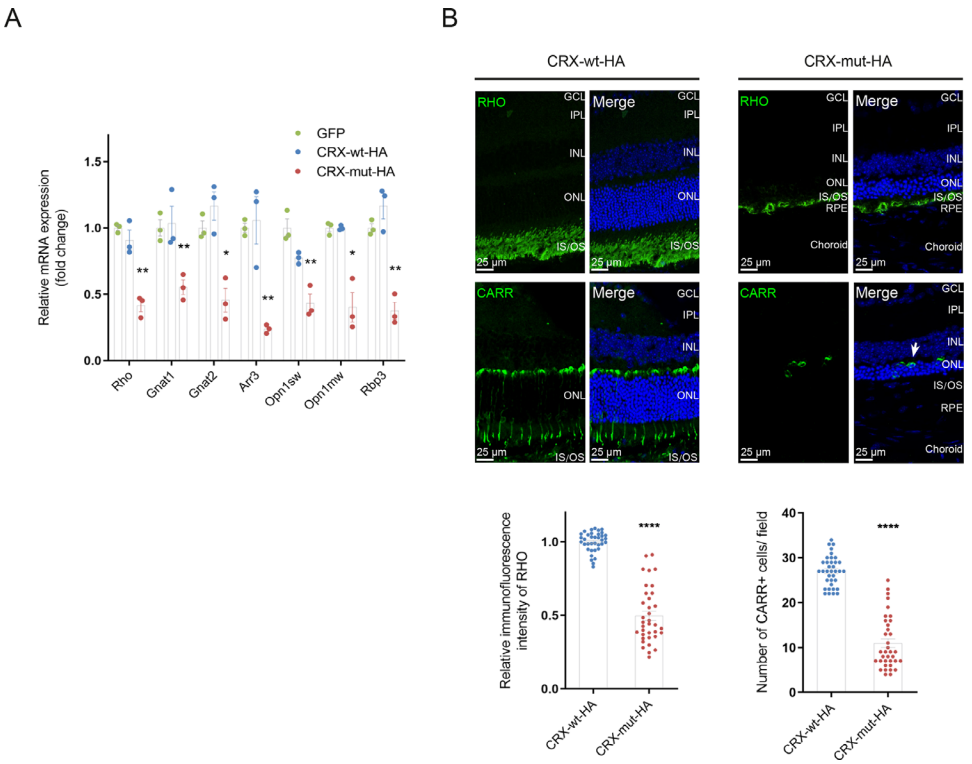

Figure 5. Expression of CRX target genes in the retinas transfected by AAV constructs. (A) The quantitative PCR analysis showed that CRX target genes were not changed in the retinas transfected by AAV-CRX-wt-HA, but significantly reduced in that transfected by AAV-CRX-mut-HA, compare to the AAV-GFP group ($n = 5$). (B) Immunostaining of RHO and cone arrestin (CARR), two target genes of CRX ($n = 36$). Six sections each with six random fields were quantified. A lower RHO immunofluorescent intensity was shown in the retinas transfected by AAV-CRX-mut-HA. CARR Immunostaining revealed the reduced number of cones and mislocalized cone nuclei in inner ONL (arrow). *$P < 0.05$, **$P < 0.01$, ***$P < 0.001$, ****$P < 0.0001$. GCL, ganglion cell layer; IPL, inner plexiform layer; INL, inner nuclear layer; IS/OS, inner segment/outer segment; RPE, retinal pigment epithelium.

using Ganzfeld ERG. AAV-CRX-wt-HA and AAV-CRX-mut-HA were injected subretinally into the left and right eyes of mice, respectively. ERG recordings showed marked decreased in the amplitudes of both dark-adapted and light-adapted responses, especially at high stimulus intensities, signifying that rod and cone photoreceptors suffered functional damage caused by mutant CRX protein (Fig. 6).

Discussion

In this study, we reported a Chinese family with autosomal-dominant CoD/CoRD caused by the c.611delC (p.S204fs) mutation in *CRX*. After identifying the c.611delC in *CRX* with sequencing and cosegregation analysis, we constructed an AAV vector carrying this variant that was delivered into the subretinal space of C57BL/6 mice to explore the pathogenesis of the mutation. The results showed the production of overexpressed truncated CRX$^{[S204fs]}$ protein and its antimorphic effect on the normal CRX protein, leading to the dysfunction and death of cone and rod photoreceptors. We developed a novel animal model by AAV-mediated gene delivery, which might be valuable for investigating the pathogenic mutation associated with CoD/CoRD and other inherited retinal dystrophies.

CoD/CoRD is heterogeneous in terms of clinical features. In this study, the phenotypes of the affected members were variable with the age of onset and severity, although carrying the same disease-causing mutation. In addition, CoD/CoRD also demonstrates a complicated underlying molecular genetic basis. There are 32 genes reported to be involved in CoD/CoRD[5]; for example, *CRX* encodes a transcription factor that regulates many photoreceptor-specific genes. To date, there are more than 80 disease-causing mutations in the *CRX* gene, spread evenly across the coding sequence, that caused a range of different retinal phenotypes according to numerous published studies.[22] The huge heterogeneity increased the difficulty of thoroughly studying the pathogenesis and exploring the therapies.

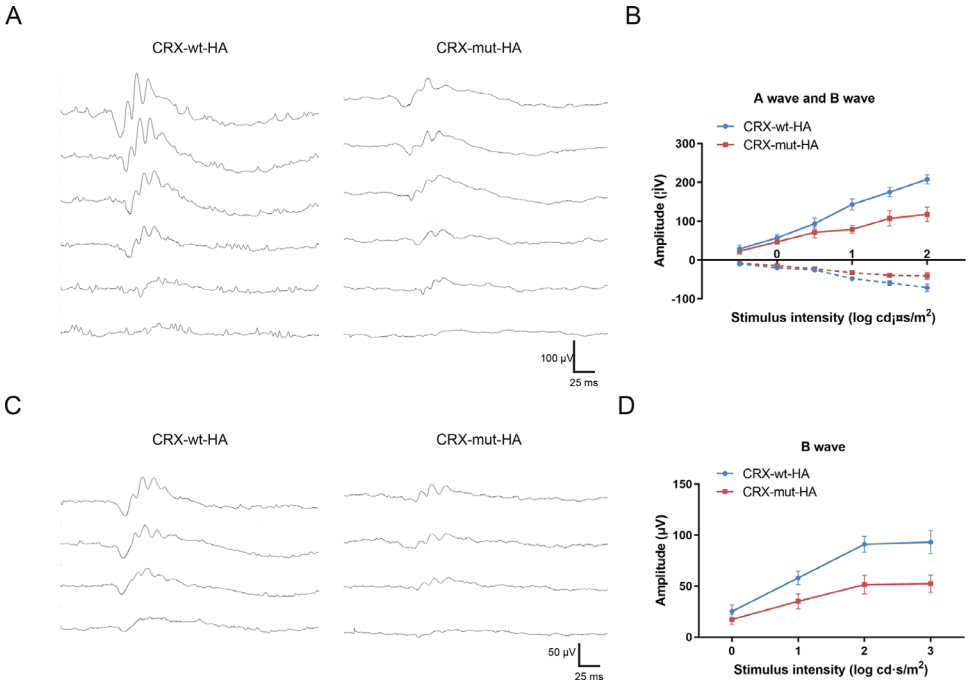

Figure 6. The retinal functional evaluation of WT mice transfected with either AAV-CRX-wt-HA or AAV-CRX-mut-HA. (A) Representative dark-adapted ERG series. (B) Dark-adapted ERG response curves. A-wave and b-wave responses are represented as dashed and solid lines, respectively. Repeated measures 2-way analysis of variance for the effect of AAV vectors: $F = 74.75$, $P < 0.0001$ for b-wave; $F = 33.05$, $P = 0.002$ for a-wave. (C) Representative light-adapted ERG series. (D) Light-adapted ERG response curves. Repeated measures 2-way analysis of variance for the effect of AAV vectors: $F = 71.35$, $^{****}P < 0.0001$. $n = 6$.

Animal models play a crucial part in understanding the pathologic mechanisms of inherited retinal dystrophies and testing novel therapeutic strategies. Knockout mouse models are established commonly to study the function of the genes related to inherited retinal dystrophies and the effect of their deletion. Additionally, several transgenic animal models carrying distinct mutations exhibit the phenotypes that accurately model the corresponding clinical features of human patients with CoD/CoRD.[6,8,11,23] The heterozygous *E168d2*/+ mice exhibited an OS defect, decreased ONL thickness, and mislocalization of cone nuclei. With regard to function, ERG recordings showed the more severely affected function of the cone than the rod in *E168d2*/+ mice.[8] However, generating transgenic mice carrying the specific mutation has the limitation of being time consuming, expensive, and labor intensive. It is well-known that AAV vectors have become a useful tool for overexpression of a protein in vivo.[24] Here, because of the conservation of CRX function and binding sequences between humans and mice,[25] and the presumable competitive antagonism of CRX$^{[S204fs]}$ on the normal CRX protein, we subretinally injected AAV-CRX-mut-HA to transfected photoreceptor cells and evaluated the changes in the retinal structure and function. The retinal structure of the model we generated was similar to that of the *E168d2*/+ mice. The ONL thickness was decreased under the influence of mutant CRX. TUNEL staining revealed the abundant apoptosis cells in mice transfected with mutant CRX, demonstrating the inability of the photoreceptor cells to maintain proper homeostasis. Immunostaining also displayed a shortened OS and abnormal cone nuclear localization. As for ERG analysis, both rod and cone photoreceptor function was damaged caused by CRX$^{[S204fs]}$. However, more severe impairment of cone function was not observed.

In terms of the underlying molecular mechanism, the c.611delC (p.S204fs) was a frameshift mutation within the transactivation domains, which might give rise to the production of antimorphic truncated CRX with abnormal transactivation activity according to the previous researches.[8,11,18] First, We found the mRNA and protein expression levels of transfected mutant CRX were two- to three-fold greater than the transfected WT CRX, with almost the same transfection efficiency. Overexpression of mutant CRX products was also observed in other frameshift mutations downstream of the homeobox domain in vitro and in vivo and conserved between human and mouse CRX,[6,8,26] probably owing to a hyperstability of the mutant mRNA.[27] Then, we detected the expression

of CRX target genes. All the tested genes were markedly decreased in mice transfected with mutant CRX compared with WT CRX or GFP at the mRNA level, and the protein level of two of them was validated by immunofluorescence staining. These findings might prove that CRX$^{[S204fs]}$ competes with the normal CRX to bind to target genes but fails to transactivate the latter, which needs further confirmation with transcription rates per cell determined.

Overall, by analyzing the results of morphology, photoreceptor gene expression, and retinal function, it is suggested that the transfection of mouse photoreceptors with AAV-CRX-mut-HA through subretinal injection proves a novel and effective research tool that reflects similar phenotypes and pathogenesis to transgenic animals carrying CRX mutation in previous studies. In addition, it can partly model the clinical features of patients with CRX-associated retinopathy, including a thinner ONL and OS, and impaired retinal function. This modeling method might be used for gain-of-function mutations in other genes that cause dominant retinal diseases. Recently, we successfully established an retinitis pigmentosa-like mouse model by subretinal injection of AAV vectors expressing mutant *RDH12*. Nevertheless, our animal model had limitations. First, it was not applicable for investigation on the development of photoreceptor cells, due to the injection of AAV constructs using 3-week-old mice. Second, it was not appropriate for loss-of-function mutations, because the hypomorphic effect cannot be revealed.

Acknowledgments

Supported by the National Natural Science Foundation of China (81730026); the National Key R&D Program (2017YFA0105301, 2019ZX09301113); Science and Technology Commission of Shanghai Municipality (17411953000, 19495800700); Shanghai Collaborative Innovation Center for Translational Medicine (TM201917); Natural Science Foundation of Shanghai (20ZR1472600); National Science Foundation of China (81700828); Interdisciplinary Program of Shanghai Jiao Tong University (ZH2018ZDA16).

Disclosure: **Y. Wang**, None; **X. Li**, None; **Y. Yang**, None; **J. Liang**, None; **Y. Liu**, None; **Y. Chen**, None; **X. Bai**, None; **J. Chen**, None; **F. Wang**, None; **X. Luo**, None; **X. Sun**, None

* YW, XL and YY contributed equally to this work.

References

1. Evans K, Duvall-Young J, Fitzke FW, Arden GB, Bhattacharya SS, Bird AC. Chromosome 19q cone-rod retinal dystrophy. Ocular phenotype. *Arch Ophthalmol.* 1995;113(2):195–201.
2. Simunovic MP, Moore AT. The cone dystrophies. *Eye (Lond).* 1998;12(Pt 3b):553–565.
3. Hamel CP. Cone rod dystrophies. *Orphanet J Rare Dis.* 2007;2(1).
4. Roosing S, Thiadens AA, Hoyng CB, Klaver CC, den Hollander AI, Cremers FP. Causes and consequences of inherited cone disorders. *Prog Retin Eye Res.* 2014;42:1–26.
5. Gill JS, Georgiou M, Kalitzeos A, Moore AT, Michaelides M. Progressive cone and cone-rod dystrophies: clinical features, molecular genetics and prospects for therapy. *Br J Ophthalmol.* 2019;103(5):711–720.
6. Ruzycki PA, Linne CD, Hennig AK, Chen S. Crx-L253X mutation produces dominant photoreceptor defects in TVRM65 mice. *Invest Ophthalmol Vis Sci.* 2017;58(11):4644–4653.
7. Ruzycki PA, Tran NM, Kefalov VJ, Kolesnikov AV, Chen S. Graded gene expression changes determine phenotype severity in mouse models of CRX-associated retinopathies. *Genome Biol.* 2015;16:171.
8. Tran NM, Zhang A, Zhang X, Huecker JB, Hennig AK, Chen S. Mechanistically distinct mouse models for CRX-associated retinopathy. *PLoS Genet.* 2014;10(2):e1004111.
9. Freund CL, Gregory-Evans CY, Furukawa T, et al. Cone-rod dystrophy due to mutations in a novel photoreceptor-specific homeobox gene (CRX) essential for maintenance of the photoreceptor. *Cell.* 1997;91(4):543–553.
10. Furukawa T, Morrow EM, Cepko CL. Crx, a novel otx-like homeobox gene, shows photoreceptor-specific expression and regulates photoreceptor differentiation. *Cell.* 1997;91(4):531–541.
11. Menotti-Raymond M, Deckman KH, David V, Myrkalo J, O'Brien SJ, Narfstrom K. Mutation discovered in a feline model of human congenital retinal blinding disease. *Invest Ophthalmol Vis Sci.* 2010;51(6):2852–2859.
12. Hu S, Du J, Chen N, et al. In vivo CRISPR/Cas9-mediated genome editing mitigates photoreceptor degeneration in a mouse model of X-linked retinitis pigmentosa. *Invest Ophthalmol Vis Sci.* 2020;61(4):31.
13. Jiang L, Frederick JM, Baehr W. RNA interference gene therapy in dominant retinitis pigmentosa

and cone-rod dystrophy mouse models caused by GCAP1 mutations. *Front Mol Neurosci.* 2014;7:25.
14. Russell S, Bennett J, Wellman JA, et al. Efficacy and safety of voretigene neparvovec (AAV2-hRPE65v2) in patients with RPE65-mediated inherited retinal dystrophy: a randomised, controlled, open-label, phase 3 trial. *Lancet.* 2017;390(10097):849–860.
15. Thakur P, Breger LS, Lundblad M, et al. Modeling Parkinson's disease pathology by combination of fibril seeds and alpha-synuclein overexpression in the rat brain. *Proc Natl Acad Sci USA.* 2017;114(39):E8284–E8293.
16. Shang Y, Yan Y, Chen B, Zhang J, Zhang T. Overexpressed MST1 impaired spatial memory via disturbing neural oscillation patterns in mice. *Genes Brain Behav.* 2020;19(6):e12678.
17. Prasad T, Zhu P, Verma A, et al. Amyloid beta peptides overexpression in retinal pigment epithelial cells via AAV-mediated gene transfer mimics AMD-like pathology in mice. *Sci Rep.* 2017;7(1):3222.
18. Tran NM, Chen S. Mechanisms of blindness: animal models provide insight into distinct CRX-associated retinopathies. *Dev Dyn.* 2014;243(10):1153–1166.
19. Liang J, She X, Chen J, et al. Identification of novel PROM1 mutations responsible for autosomal recessive maculopathy with rod-cone dystrophy. *Graefes Arch Clin Exp Ophthalmol.* 2019;257(3):619–628.
20. Guo Y, Gao M, Wan X, et al. An improved method for establishment of murine retinal detachment model and its 3D vascular evaluation. *Exp Eye Res.* 2020;193:107949.
21. Sun J, Huang P, Liang J, et al. Cooperation of Rel family members in regulating Abeta1-40-mediated pro-inflammatory cytokine secretion by retinal pigment epithelial cells. *Cell Death Dis.* 2017;8(10):e3115.
22. Yi Z, Xiao X, Li S, Sun W, Zhang Q. Pathogenicity discrimination and genetic test reference for CRX variants based on genotype-phenotype analysis. *Exp Eye Res.* 2019;189:107846.
23. Jiang L, Li TZ, Boye SE, Hauswirth WW, Frederick JM, Baehr W. RNAi-mediated gene suppression in a GCAP1(L151F) cone-rod dystrophy mouse model. *PLoS One.* 2013;8(3):e57676.
24. Trapani I, Auricchio A. Seeing the light after 25 years of retinal gene therapy. *Trends Mol Med.* 2018;24(8):669–681.
25. Cai X, Conley SM, Cheng T, Al-Ubaidi MR, Naash MI. A 350 bp region of the proximal promoter of Rds drives cell-type specific gene expression. *Exp Eye Res.* 2010;91(2):186–194.
26. Nichols LL, 2nd, Alur RP, Boobalan E, et al. Two novel CRX mutant proteins causing autosomal dominant Leber congenital amaurosis interact differently with NRL. *Hum Mutat.* 2010;31(6):E1472–1483.
27. Inez Oh XZ, Tran Nicholas, Chen Shiming. Hyperstability of mutant mRNA causes pathogenic overexpression of mutant CRX in autosomal dominant retinopathies. *Invest Ophthalmol Vis Sci.* 2017;58(8):3590.